Electronic Supplementary Material (ESI) for Environmental Science: Nano.

Electronic supplementary information

Probing the effects of redox conditions and dissolved Fe^{2+} on nanomagnetite stoichiometry by wet chemistry, XRD, XAS and XMCD

Phoomipat Jungcharoen[1], Mathieu Pédrot[1], Fadi Choueikani[2], Mathieu Pasturel[3], Khalil Hanna[4], Frank Heberling[5], Marawit Tesfa[1], Rémi Marsac[1]*

[1] Univ Rennes, CNRS, Géosciences Rennes – UMR 6118, F-35000 Rennes, France.
E-mail: remi.marsac@univ-rennes1.fr

[2] Synchrotron SOLEIL, L'ormes des Merisiers, Saint Aubin BP48, 91192 Gif sur Yvette cedex, France.

[3] Univ Rennes, CNRS, ISCR – UMR 6226, F-35000, Rennes, France

[4] Univ Rennes, Ecole Nationale Supérieure de Chimie de Rennes, CNRS, ISCR-UMR 6226, F-35000, Rennes, France.

[5] Institut für Nukleare Entsorgung, Karlsruhe Institute of Technology, P.O. Box 3640, D-76021 Karlsruhe, Germany

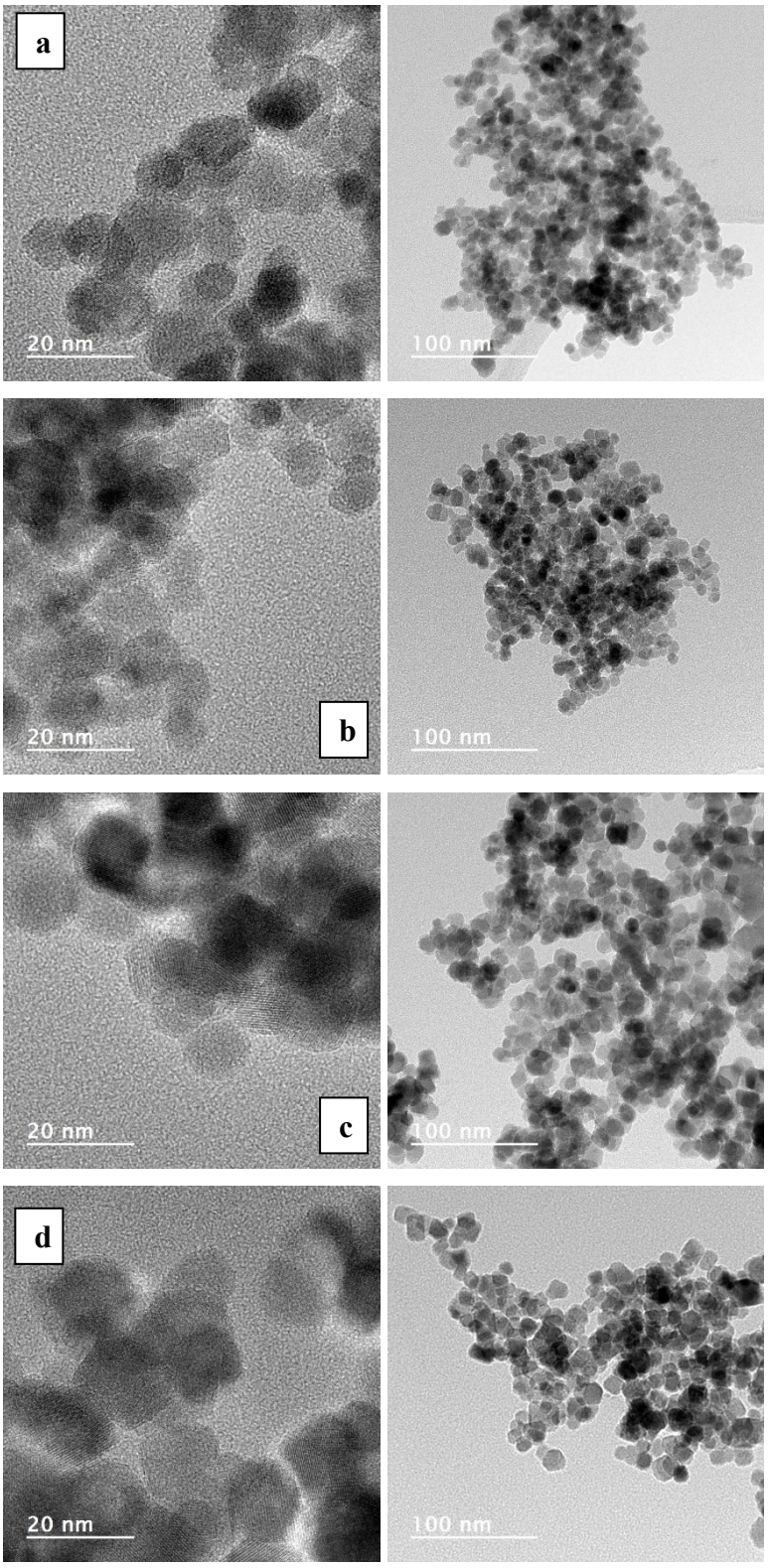
a
20 nm
100 nm
20 nm
b
100 nm
20 nm
c
100 nm
d
20 nm
100 nm

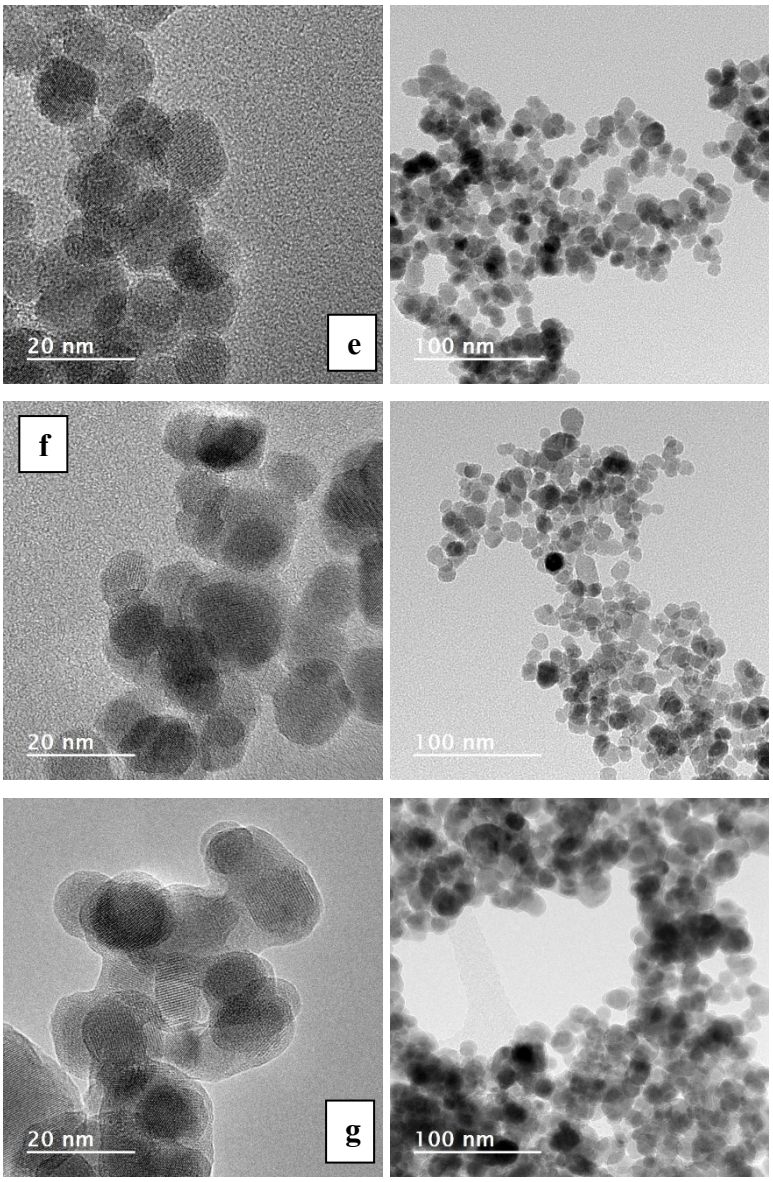

Figure S1. TEM images of synthetic magnetite nanoparticles with various stoichiometries ((a) R0.1, (b) R0.2, (c) R0.3, (d) R0.4, (e) R0.5), (f) the addition of Fe(II) to R0.1 to reach R = 0.5, and (g) overloading of R0.5 with 2500 μM Fe(II).

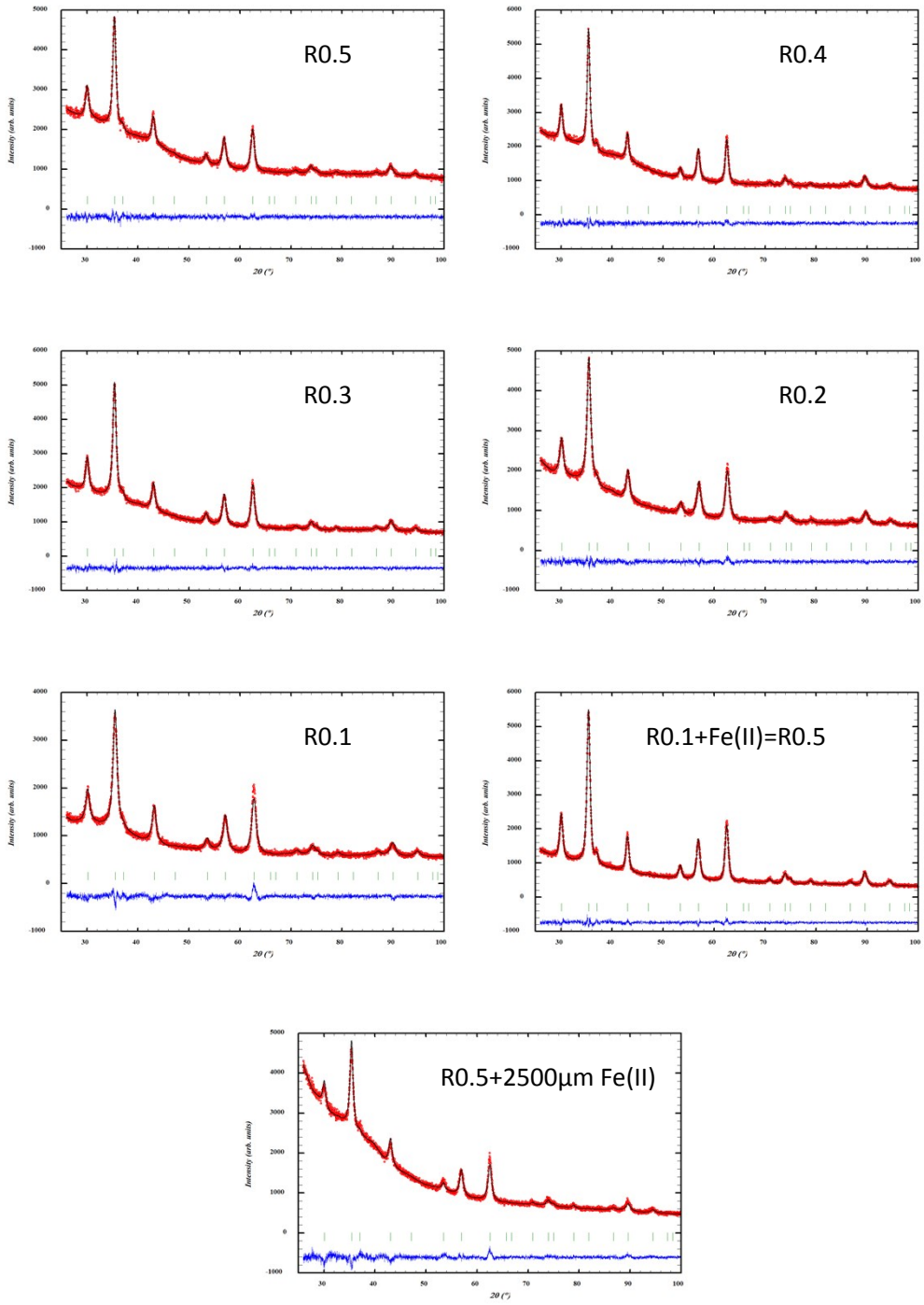

Figure S2. Selected angular domain of the Rietveld refined XRD patterns of the different magnetite samples presented in Table S1. The experimental diffractograms are plotted in red symbols, the calculated pattern in black line, and the difference between them as lower blue line. The vertical ticks indicate the Bragg peak positions for the cubic magnetite structure. The strong background observed below 60° is due to the glycerol used to protect the powders against oxidation in air.

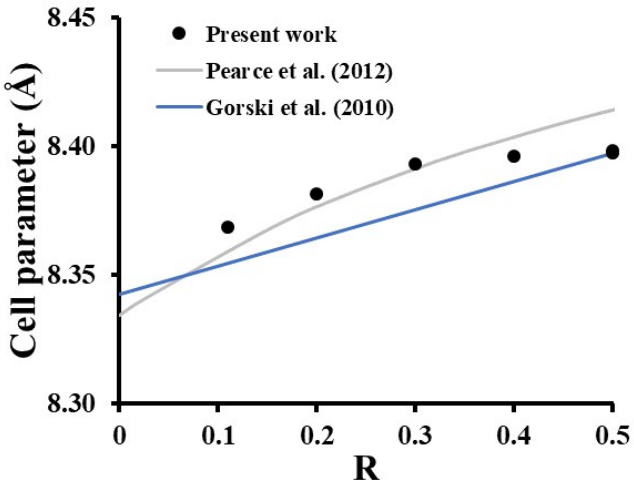

Figure S3. Cell parameter versus magnetite stoichiometry (R). Presently measure values are compared with calculated ones in previous studies.[30,38]

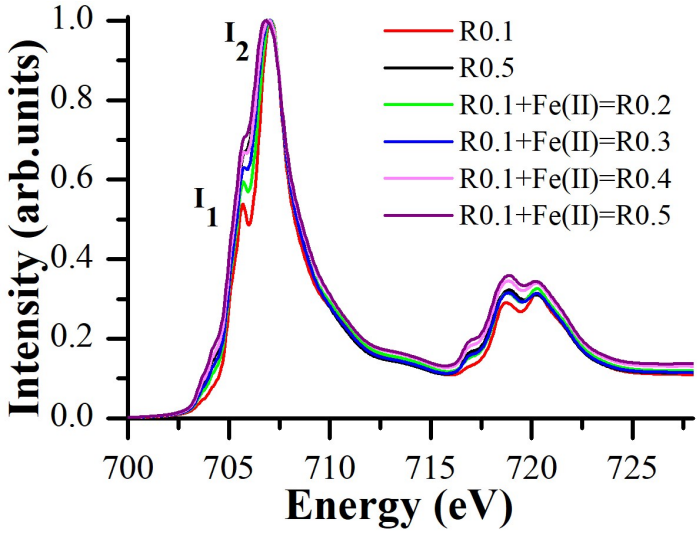

Figure S4. Isotropic XAS of the dissolved Fe^{2+} addition on non-stoichiometric magnetite (R0.1) to increase the stoichiometry at pH 8, and measured at B= 6 T and T=4 K at the Fe-$L_{2,3}$-edge.

Table S1. Effective Fe(II)/Fe(III) ratio R_{eff} obtained from chemical analysis, cell parameter and Crystallite size from XRD pattern refinements, average particle size by TEM and determined S value by XMCD for stoichiometric nanomagnetite (R0.5), oxidized products (R0.1 to R0.4), recharged sample (R0.1 + Fe(II) = R0.5) and overloaded samples (R0.5 + 250-2500 µM Fe(II)). "nd" means "non-determined".

Sample	R_{eff} in solid phase	Cell parameter (Å)	Crystallite size by XRD (nm)	Particle size by TEM (nm)	S value
R0.1	0.11	8.3685(4)	6.3	9.6±2.3	0.87
R0.2	0.20	8.3814(3)	7.1	8.9±2.1	0.95
R0.3	0.30	8.3932(3)	7.7	10.6±2.3	1.06
R0.4	0.40	8.3964(3)	9.4	11.1±2.0	1.14
R0.5	0.50	8.3976(4)	8.0	11.5±1.5	1.15
R0.1+Fe(II)=R0.5	0.50	8.3983(2)	9.0	11.3±2.0	1.19
R0.5+250 µM Fe(II)	0.54	nd	nd	nd	1.16
R0.5+500 µM Fe(II)	0.58	nd	nd	nd	1.17
R0.5+1000 µM Fe(II)	0.65	nd	nd	nd	1.22
R0.5+2500µM Fe(II)	0.932	8.3951(5)	8.3	12.9±1.8	1.17

Table S2. Literature values of the S ratio of magnetite and maghemite nanoparticles and methods of syntheses.

References	$S_{magnetite}$	$S_{maghemite}$	Sizes and methods of synthesis
This study	1.15	-	10 nm. Co-precipitation in NaOH
1	1.15	0.69	4 nm. Thin film
2	1.15	-	10 nm. Co-precipitation in NH_4OH. Sample at pH8
3	1.30	0.65	5-22 nm. Thermal decomposition
4	1.30	0.68	9 nm. Thermal decomposition

5	1.30	-	31 ± 7.2 nm. Biogenic magnetite
6	1.35	-	20-30 nm. Biogenic magnetite
7	1.46	0.76	5-13 nm. Iron/iron oxide granular nanostructures obtained by cold compacting core-shell nanoparticles
8	1.42	0.75	12 nm. Iron-iron oxide nanostructured under frozen state at low temperature

References

1 E. Pellegrin, M. Hagelstein, S. Doyle, H. O. Moser, J. Fuchs, D. Vollath, S. Schuppler, M. A. James, S. S. Saxena, L. Niesen, O. Rogojanu, G. A. Sawatzky, C. Ferrero, M. \ Borowski, O. Tjernberg and N. B. Brookes, Characterization of Nanocrystalline g-Fe2O3 with Synchrotron Radiation Techniques, 1999, **215**, 797–801.

2 H. Peng, C. I. Pearce, W. Huang, Z. Zhu, A. T. N'Diaye, K. M. Rosso and J. Liu, Reversible Fe(II) uptake/release by magnetite nanoparticles, *Environ. Sci.: Nano*, 2018, **5**, 1545–1555.

3 J. Park, K. An, Y. Hwang, J.-G. Park, H.-J. Noh, J.-Y. Kim, J.-H. Park, N.-M. Hwang and T. Hyeon, Ultra-large-scale syntheses of monodisperse nanocrystals, *Nature Mater*, 2004, **3**, 891–895.

4 A. Kuzmin and J. Chaboy, EXAFS and XANES analysis of oxides at the nanoscale, *IUCrJ*, 2014, **1**, 571–589.

5 C. Carvallo, P. Sainctavit, M.-A. Arrio, N. Menguy, Y. Wang, G. Ona-Nguema and S. Brice-Profeta, Biogenic vs. abiogenic magnetite nanoparticles: A XMCD study, *American Mineralogist*, 2008, **93**, 880–885.

6 V. S. Coker, C. I. Pearce, R. A. D. Pattrick, G. van der Laan, N. D. Telling, J. M. Charnock, E. Arenholz and J. R. Lloyd, Probing the site occupancies of Co-, Ni-, and Mn-substituted biogenic magnetite using XAS and XMCD, *American Mineralogist*, 2008, **93**, 1119–1132.

7 L. Signorini, L. Pasquini, F. Boscherini, E. Bonetti, I. Letard, S. Brice-Profeta and P. Sainctavit, Local magnetism in granular iron/iron oxide nanostructures by phase- and site-selective x-ray magnetic circular dichroism, *Phys. Rev. B*, 2006, **74**, 014426.

8 F. Jiménez-Villacorta, C. Prieto, Y. Huttel, N. D. Telling and G. van der Laan, X-ray magnetic circular dichroism study of the blocking process in nanostructured iron-iron oxide core-shell systems, *Phys. Rev. B*, 2011, **84**, 172404.